Partial substitution with significant effect: coexistence of wide band gap and large birefringence in oxychalcogenide $AEGe_2O_4Se$ (AE = Sr, Ba)

Mao-Yin Ran,[a,b,c] Sheng-Hua Zhou,[a,b,c] Wen-Bo Wei,[a,b,c] A-Yang Wang,[a,b,d] Xin-Tao Wu,[a,b] Hua Lin,[*a,b] and Qi-Long Zhu[*a,b]

[a]*State Key Laboratory of Structural Chemistry, Fujian Institute of Research on the Structure of Matter, Chinese Academy of Sciences, Fuzhou 350002, China*

[b]*Fujian Science & Technology Innovation Laboratory for Optoelectronic Information of China, Fuzhou, Fujian 350108, China*

[c]*University of Chinese Academy of Sciences, Beijing 100049, China*

[d]*College of Chemistry, Fuzhou University, Fujian 350002, China*

*E-mail: linhua@fjirsm.ac.cn and qlzhu@fjirsm.ac.cn.

Table of Contents

Figure S3. Comparison of calculated formation enthalpies between $AEGe_2O_4Se$ (AE = Sr, Ba) and reported oxyselenides.

Figure S4. The experimental (red) and simulated (black) PXRD of (a) $SrGe_2O_4Se$; (b) $BaGe_2O_4Se$.

Figure S5. The characterizations of $SrGe_2O_4Se$: (a) EDX results and (b) SEM image and corresponding elemental mapping analysis.

Figure S6. The characterizations of $BaGe_2O_4Se$: (a) EDX results and (b) SEM image and corresponding elemental mapping analysis.

Figure S7. The TG-DTA curves of (a) $SrGe_2O_4Se$ and (b) $BaGe_2O_4Se$.

Table S1. Atomic coordinates and equivalent isotropic displacement parameters of $AEGe_2O_4Se$ (AE = Sr, Ba).

Table S2. Selected bond lengths (Å) and angle (°) of $SrGe_2O_4Se$.

Table S3. Selected bond lengths (Å) and angle (°) of $BaGe_2O_4Se$.

Table S4. Properties comparison between energy gap and birefringence of the reported oxychalcogenides.

4 References

1 Experimental Section

1.1 Materials and Instruments

All reagents used in the present experiments were purchased from commercial sources and directly used without further purification. All weighing processes were completed in an anhydrous and oxygen-free glove box. The semi-quantitative energy dispersive X-ray (EDX, Oxford INCA) spectra were measured with a field emission scanning electron microscope (FESEM, JSM6700F). Powder X-ray diffraction (XRD) analysis was carried out in a Rigaku Mini-Flex II powder diffractometer (Cu-K_α, λ = 1.5418 Å). UV-vis-NIR absorption measurement was performed in the region of 200−2500 nm at room temperature using an UV-vis-NIR spectrometer (Perkin-Elmer Lambda 950). The reflectance spectrum of the $BaSO_4$ powder was collected as the baseline and the diffuse reflectance data were converted to absorbance internally by the instrument by use of the Kubelka-Munk function.[1] The thermal stability analyses were measured on a NETZSCH STA 449C simultaneous analyser.

1.2 Synthesis

The crystals of $AEGe_2O_4Se$ (AE = Sr, Ba) were synthesized with a high yield of 60% based on Ge) through a high-temperature solid-state reaction. The raw materials, including 1 mmol Sr (0.088 g), 1 mmol Ba (0.137 g), 1 mmol Se (0.079 g), and 2 mmol GeO_2 (0.210 g), were ground to a consistent mixture without further purification. The mixture was then heated from room temperature to 673 K. After holding at 673 K for 10 hours, the temperature was raised to 1223 K in 30 hours. The furnace was kept at the highest temperature for 100 hours and then gradually cooled down to 523 K within 150 hours. Finally, the crystals were brought back to room temperature naturally without any additional heating. After washing the crystals with

deionized water and ethanol, the $AEGe_2O_4Se$ (AE = Sr, Ba) were obtained. These crystals remained stable in both air and moisture. To determine the crystal structure, a selection of high-quality single crystals of $AEGe_2O_4Se$ (AE = Sr, Ba) were made.

1.3 Birefringence Measurements

The birefringence (Δn) was characterized by using the polarizing microscope (ZEISS Axio Scope, A1) equipped with Berek compensator. The wavelength of the light source was 546 nm. The formula for calculating the Δn is $R = | N_e – N_o | \times T = \Delta n \times T$. Here, R represents the optical path difference and T denotes the thickness of the crystal.

1.4 Single-Crystal Structure determination

Taking some high-quality crystals of $AEGe_2O_4Se$ (AE = Sr, Ba) with suitable sizes were selected for single-crystal X-ray diffraction (XRD) analysis. The single-crystal diffraction data collections were collected on a Saturn 724 install with graphite-monochromated Mo-K_α radiation (λ = 0.71073 Å) at room temperature.The absorption correction was performed by the multi-scan method.[2] Using direct methods and maken further refinement by full-matrix least-square fitting on F^2 based on *SHELX−2014* software, the precise struture was determined sussessfully.[3] Crystal data and structure refinement parameters were given in Table 1. The final refined atomic positions and isotropic thermal parameters are listed in Table S1. Interatomic distances (Å) and bond angles (deg) are displayed in Table S2 and Table S3. CIFs of $AEGe_2O_4Se$ (AE = Sr, Ba) have been submitted with CCDC numbers 2301111 and 2301112.

2 Computational Details

The DFT calculations have been performed using the *Vienna ab initio simulation package* (VASP)[4–6] with the Perdew-Burke-Ernzerhof (PBE)[7] exchange correlation functional. The projected augmented wave (PAW)[8] potentials with the valence states 4d, 5p and 6s for Ba, 3d, 4p and 5s for Sr, 4s and 4p for Ge, 4s and 4p for Se, 2s and 2p for O respectively, have been used. A Γ-centered 7×7×9 Monkhorst-Pack grid for the Brillouin zone sampling[9] and a cutoff energy of 900 eV for the plane wave expansion were found to get convergent lattice parameters.

3 Figures and Tables

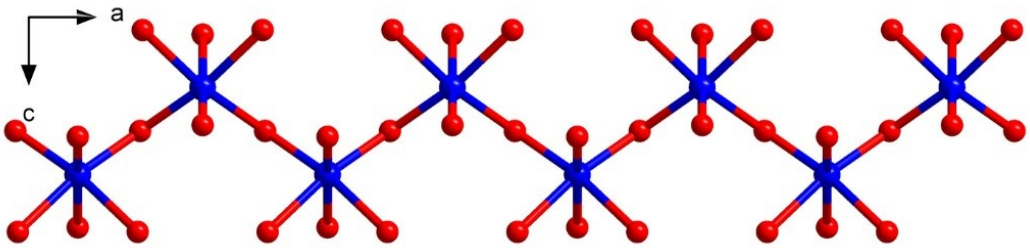

Figure S1. 1D chain in $BaGe_2O_5$ viewed from *b* direction.

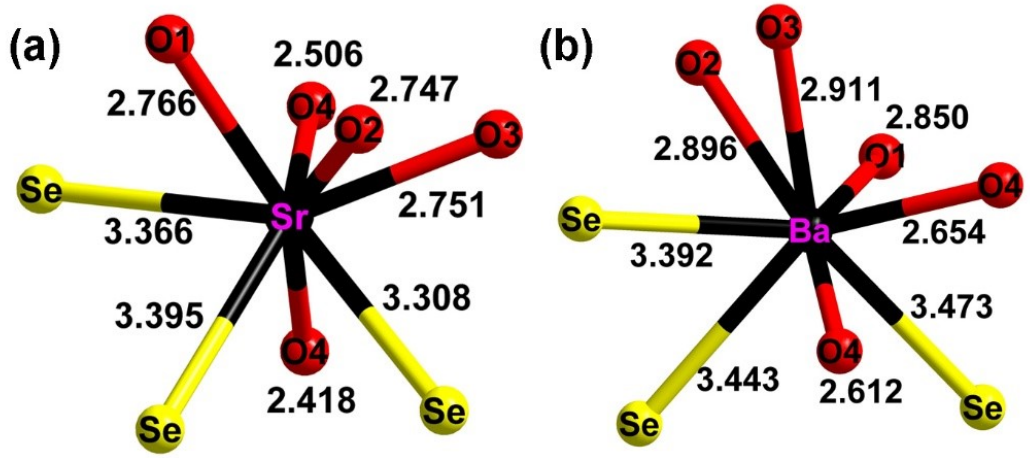

Figure S2. Coordination environments and bond distances of the AE atoms in (a) $SrGe_2O_4Se$; (b) $BaGe_2O_4Se$.

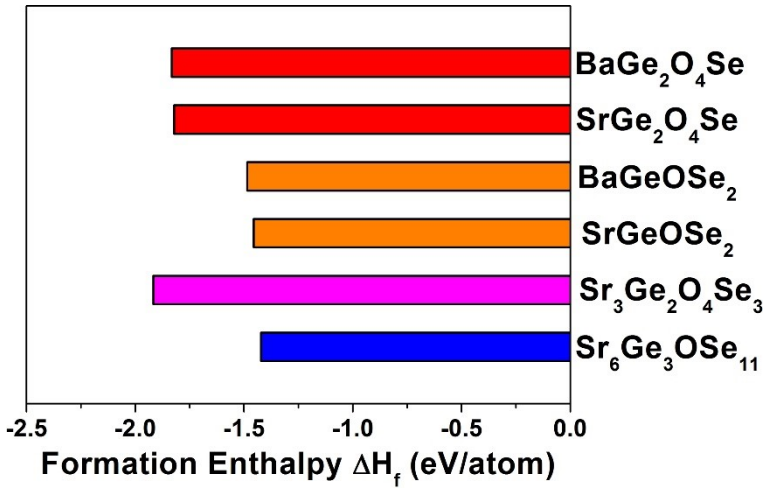

Figure S3. Comparison of calculated formation enthalpies between $AEGe_2O_4Se$ (AE = Sr, Ba) and reported oxyselenides.

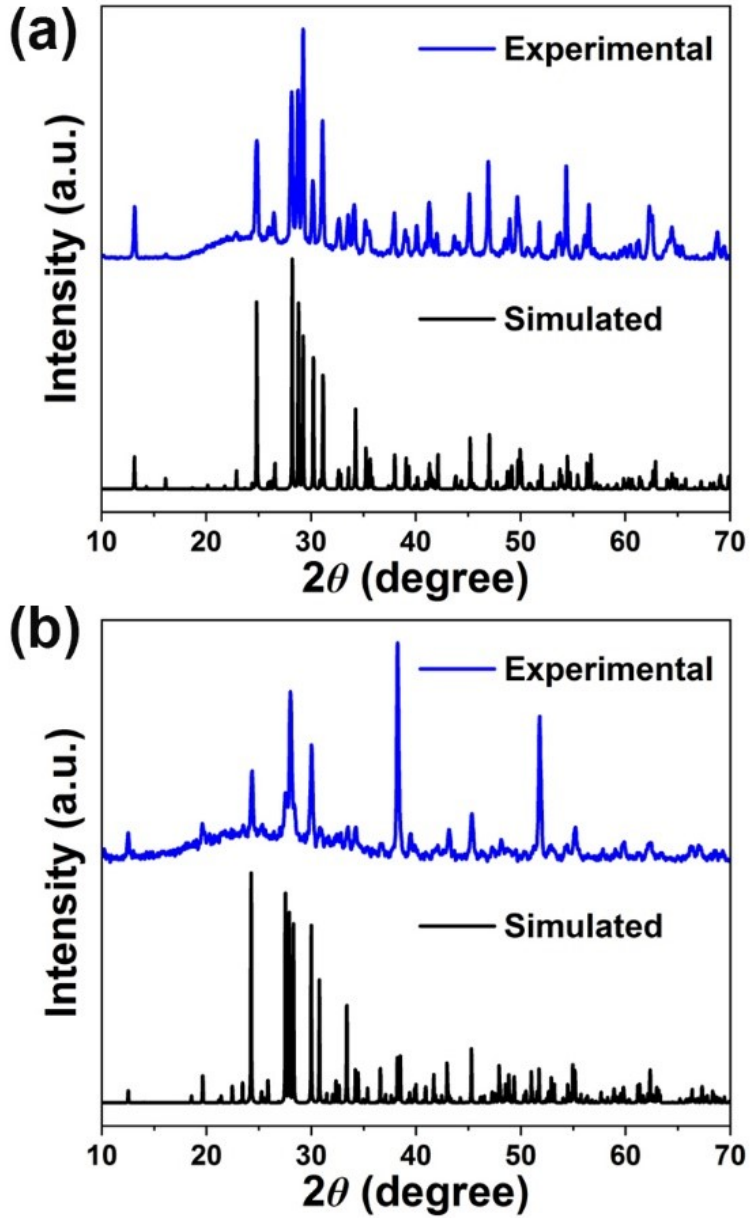

Figure S4. The experimental (red) and simulated (black) PXRD of (a) $SrGe_2O_4Se$; (b) $BaGe_2O_4Se$.

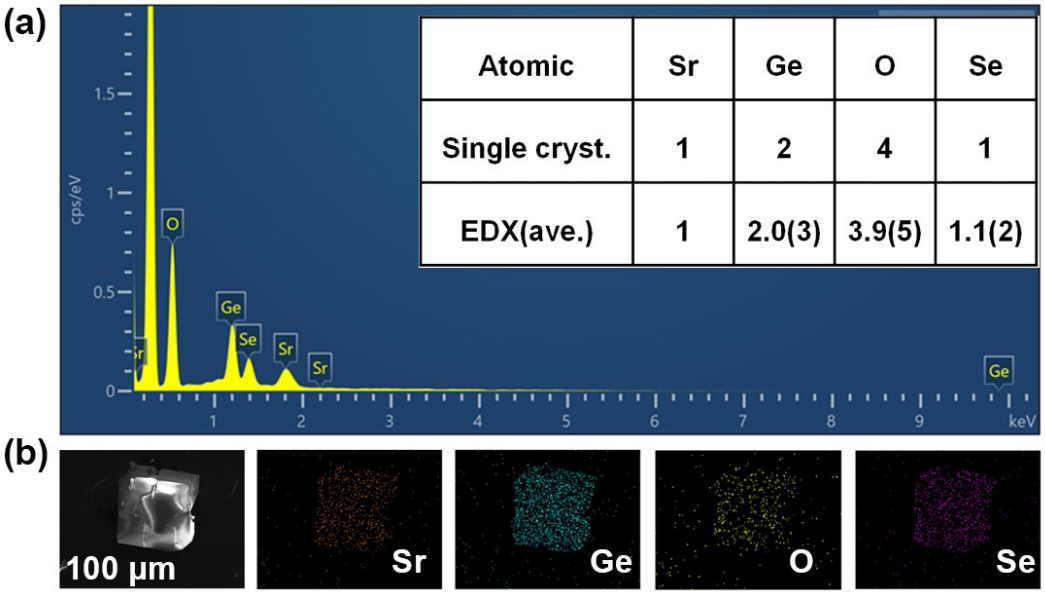

Atomic	Sr	Ge	O	Se
Single cryst.	1	2	4	1
EDX(ave.)	1	2.0(3)	3.9(5)	1.1(2)

Figure S5. The characterizations of $SrGe_2O_4Se$: (a) EDX results and (b) SEM image and corresponding elemental mapping analysis.

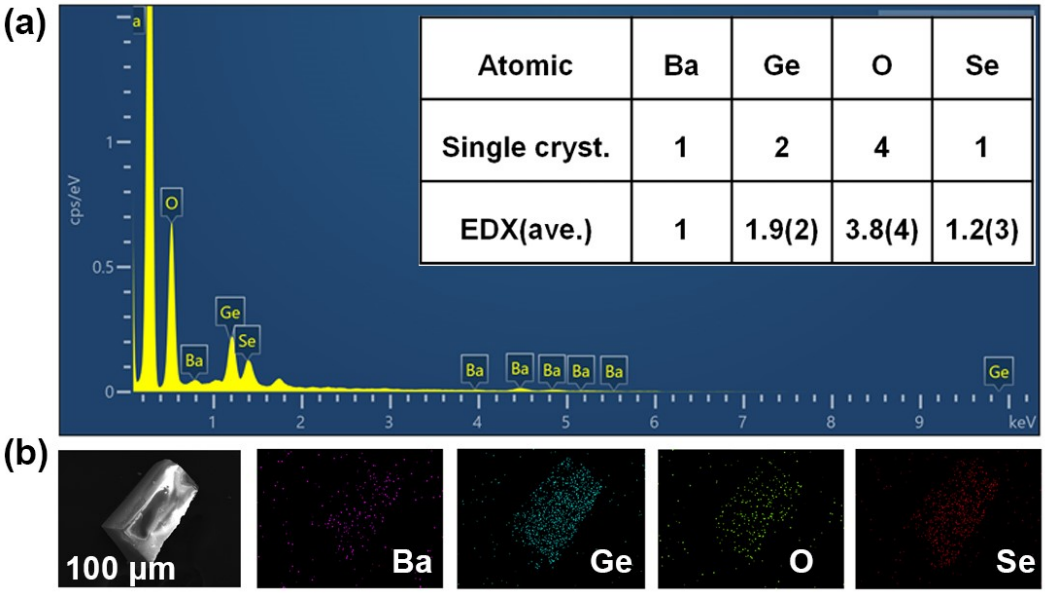

Atomic	Ba	Ge	O	Se
Single cryst.	1	2	4	1
EDX(ave.)	1	1.9(2)	3.8(4)	1.2(3)

Figure S6. The characterizations of $BaGe_2O_4Se$: (a) EDX results and (b) SEM image and corresponding elemental mapping analysis.

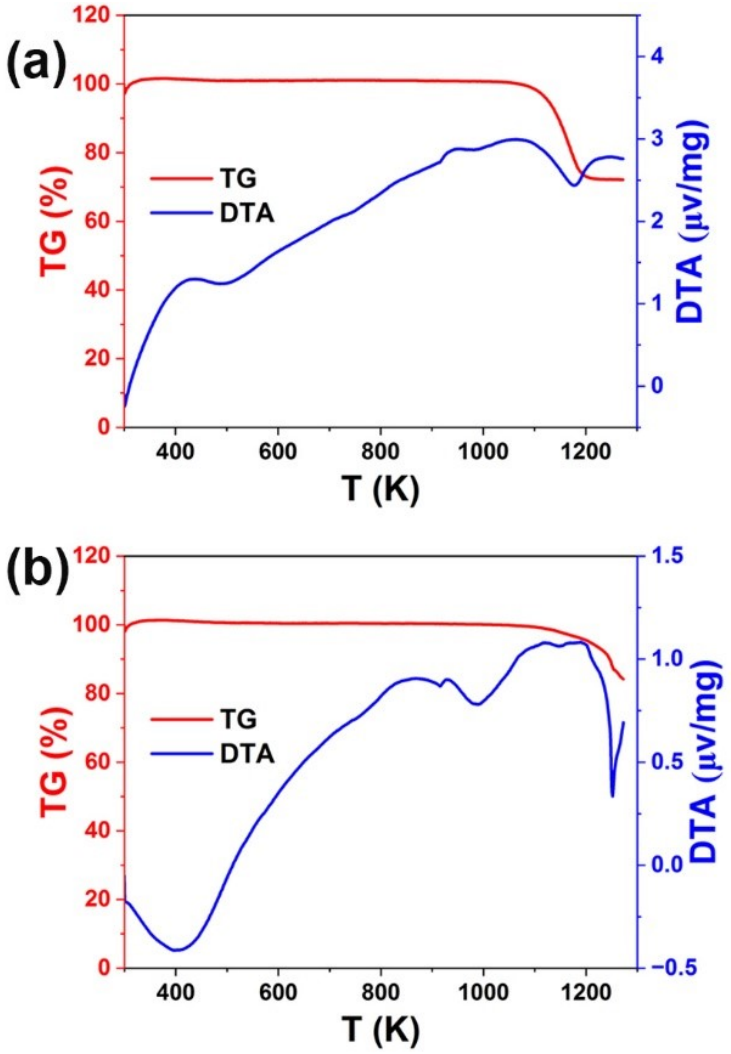

Figure S7. The TG-DTA curves of (a) $SrGe_2O_4Se$ and (b) $BaGe_2O_4Se$.

Table S1. Atomic coordinates and equivalent isotropic displacement parameters of $AEGe_2O_4Se$ (AE = Sr, Ba)

atom	wyckff	x	y	z	U_{eq}(Å)^2
		$SrGe_2O_4Se$			
Sr	4*e*	0.15152(17)	0.42724(12)	0.32767(14)	0.0093(3)
Ge1	4*e*	0.58321(18)	0.29599(13)	0.04044(15)	0.0040(3)
Ge2	4*e*	0.3731(2)	0.06411(16)	0.23593(19)	0.0171(4)
O1	4*e*	0.3741(12)	0.1865(9)	0.3930(10)	0.0072(17)
O2	4*e*	0.5048(12)	0.4130(9)	0.1910(10)	0.0081(18)
O3	4*e*	0.5511(12)	0.1233(8)	0.1131(10)	0.0072(18)
O4	4*e*	0.1542(13)	0.0475(9)	0.1309(11)	0.0103(18)
Se	4*e*	0.11214(18)	0.66243(13)	0.03025(15)	0.0093(3)
		$BaGe_2O_4Se$			
Ba	4*e*	0.14733(7)	0.42205(5)	0.32121(6)	0.0057(2)
Ge1	4*e*	0.58085(12)	0.29660(9)	0.04454(11)	0.0036(3)
Ge2	4*e*	0.37660(14)	0.06600(10)	0.23770(13)	0.0114(3)
O1	4*e*	0.3797(8)	0.1834(6)	0.3987(7)	0.0059(13)
O2	4*e*	0.5124(8)	0.4102(6)	0.1966(7)	0.0055(13)
O3	4*e*	0.5484(9)	0.1250(6)	0.1150(7)	0.0066(12)
O4	4*e*	0.1618(9)	0.0596(6)	0.1369(8)	0.0083(13)
Se	4*e*	0.12829(11)	0.66459(9)	0.02589(10)	0.0059(3)

U_{eq} is defined as one third of the trace of the orthogonalized U_{ij} tensor.

Table S2. Selected bond lengths (Å) and angle (°) of $SrGe_2O_4Se$.

Ge1–O1	1.777(8)	∠O2–Ge1–O3	107.1(4)
Ge1–O2	1.783(8)	∠O1–Ge1–Se	120.0(3)
Ge1–O3	1.770(8)	∠O2–Ge1–Se	114.5(3)
Ge1–Se	2.2323(18)	∠O3–Ge1–Se	113.5(3)
Ge2–O1	1.741(9)		
Ge2–O2	1.737(9)	∠O1–Ge2–O2	109.3(4)
Ge2–O3	1.744(9)	∠O1–Ge2–O3	105.3(4)
Ge2–O4	1.645(9)	∠O1–Ge2–O4	112.9(4)
		∠O2–Ge2–O3	97.9(4)
∠O1–Ge1–O2	98.1(4)	∠O2–Ge2–O4	118.3(4)
∠O1–Ge1–O3	101.6(4)	∠O3–Ge2–O4	111.5(4)

Table S3. Selected bond lengths (Å) and angle (°) of $BaGe_2O_4Se$.

Ge1–O1	1.792(6)	∠O2–Ge1–O3	105.7(3)
Ge1–O2	1.783(6)	∠O1–Ge1–Se	119.4(2)
Ge1–O3	1.768(6)	∠O2–Ge1–Se	114.6(2)
Ge1–Se	2.2365(12)	∠O3–Ge1–Se	113.5(2)
Ge2–O1	1.759(6)		
Ge2–O2	1.748(6)	∠O1–Ge2–O2	109.3(3)
Ge2–O3	1.771(6)	∠O1–Ge2–O3	107.0(3)
Ge2–O4	1.666(6)	∠O1–Ge2–O4	110.8(3)
		∠O2–Ge2–O3	98.1(3)
∠O1–Ge1–O2	99.8(3)	∠O2–Ge2–O4	119.2(3)
∠O1–Ge1–O3	101.9(3)	∠O3–Ge2–O4	111.2(3)

Table S4. Properties comparison between energy gap and birefringence of the reported oxychalcogenides.

Number	Compounds	Space group	E_g (eV)	Δn (cal)	Ref.
1	$Ba_6Sb_6O_2S_{13}$	$P2_1/c$ (No. 14)	1.68	0.66	10
2	Eu_3GeOS_4	$Pca2_1$ (No. 29)	2.05	0.02	11
3	$Ba_3Ge_2O_4Te_3$	$R3m$ (No. 160)	2.08	0.14	12
4	$Sr_2FeGe_2OS_6$	$P\bar{4}2_1m$ (No. 113)	2.24	0.127	13
5	$Sr_3Ge_2O_4Te_3$	$R3m$ (No. 160)	2.26	0.152	14
6	$La_3OSCl_2[SbS_3]$	$P6_3mc$ (No. 186)	2.5	0.269	15
7	$Sr_3[VO_4][GaSe_3]$	$P2_1/c$ (No. 14)	2.51	0.025	16
8	$Sr_3[VO_4][InSe_3]$	$Pmc2_1$ (No. 26)	2.62	0.028	16
9	$Ba_2SnSSi_2O_7$	$P4bm$ (100)	2.70	0.082	17
10	$Sr_2CoGe_2OS_6$	$P\bar{4}2_1m$ (No. 113)	2.77	0.09	18
11	$Sr_3Ge_2O_4Se_3$	$R3m$ (No. 160)	2.96	0.058	19
12	$Ca_2GeGa_2OS_6$	$P\bar{4}2_1m$ (No. 113)	3.15	0.13	20
13	$Sr_2GeGa_2OS_6$	$P\bar{4}2_1m$ (No. 113)	3.15	0.11	20
14	$SrGeOSe_2$	$P2_12_12_1$ (No. 19)	3.16	0.16	21
15	$BaGeOSe_2$	$P2_12_12_1$ (No. 19)	3.2	0.153	22
16	$LaSrGa_3OS_6$	$P\bar{4}2_1m$ (No. 113)	3.21	0.099	23
17	$[GeOSe_3]SeBa_3$	$Pca2_1$ (No. 29)	3.25	0.030	24
18	$[GeOSe_3]SeSr_3$	$Pca2_1$ (No. 29)	3.25	0.035	24
19	$LaCaGa_3OS_6$	$P\bar{4}2_1m$ (No. 113)	3.27	0.134	23
20	$Ba_3MnGe_3O_2S_8$	$P2_1/c$ (No. 14)	3.39	0.06	25
21	$Sr_3[SnOSe_3][CO_3]$	$Pmn2_1$ (No. 31)	3.46	0.12	26
22	$Sr_2MnGe_2OS_6$	$P\bar{4}2_1m$ (No. 113)	3.51	0.064	27
23	$Sr_2ZnSn_2OS_6$	$P\bar{4}2_1m$ (No. 113)	3.52	0.12	28
24	$[GeOS_3]SBa_3$	$Pca2_1$ (No. 29)	3.53	0.017	24
25	$SrGe_2O_4Se$	$P2_1/c$ (No. 14)	3.57	0.238	**This work**
26	$Sr_2CdGe_2OS_6$	$P\bar{4}2_1m$ (No. 113)	3.62	0.193	27
27	$K_2Ba_{0.5}Ga_9O_2S_{13}$	$P\bar{6}$ (No. 168)	3.72	0.078	29
28	$Sr_2ZnGe_2OS_6$	$P\bar{4}2_1m$ (No. 113)	3.73	0.114	27

29	$BaGe_2O_4Se$	$P2_1/c$ (No. 14)	3.81	0.209	**This work**
30	$Ba_3CdGe_3O_2S_8$	$P2_1/c$ (No. 14)	3.82	0.15	25
31	$[GeOS_3]SBa_3$	$Pca2_1$ (No. 29)	3.88	0.031	24
32	$Ba_2SnSSi_2O_7$	$P4bm$ (No. 100)	4.05	0.105	30
33	$Nd_3[Ga_3O_3S_3][Ge_2O_7]$	$P\bar{6}2c$ (No. 190)	4.35	0.091	31
34	$SrGeOS_2$	$P2_12_12_1$ (No. 19)	4.36	0.135	32
35	$BaGeOS_2$	$P2_12_12_1$ (No. 19)	4.43	0.121	32
36	$[Ba_2F_2][Ge_2O_3S_2]$	$Aba2$ (No. 41)	4.45	0.079	33
37	$La_3Ga_3Ge_2S_3O_{10}$	$P\bar{6}2c$ (No. 190)	4.7	0.11	34

4 References

[1] P. Kubelka, An article on optics of paint layers, *Z. Tech. Phys.*, 1931, **12**, 593–601.

[2] CrystalClear Version 1.3.5; Rigaku Corp.: Woodlands, TX, 1999.

[3] G. M. Sheldrick, A short history of SHELX, *Acta Crystallogr., Sect. A: Found. Crystallogr.* 2008, 112–122.

[4] G. Kresse, VASP, 5.3.5; http://cms.mpi.univie.ac.at/vasp/vasp/vasp.html.

[5] G. Kresse and J. Furthmuller, Efficient iterative schemes for ab initio total-energy calculations using a plane-wave basis set. *Phys. Rev. B: Condens. Matter,* 1996, **54**, 11169–11186.

[6] G. Kresse and D. Joubert, From ultrasoft pseudopotentials to the projector augmented-wave method. *Phys. Rev. B: Condens. Matter,* 1999, **59**, 1758–1775.

[7] P. E. Blochl, Projector augmented-wave method. *Phys. Rev. B: Condens. Matter* ,1994, **54**, 17953–17979.

[8] J. P. Perdew, K. Burke and M. Ernzerhof, Generalized Gradient Approximation Made Simple. *Phys. Rev. Lett.,* 1996, **77**, 3865–3868.

[9] D. J. Chadi, Special points for Brillouin-zone integrations. *Phys. Rev. B: Condens. Matter,* 1976, **16**, 1746–1747.

[10] Y. Shi, S. Zhou, P. Liu, X. Wu, H. Lin and Q. Zhu, Unique $[Sb_6O_2S_{13}]^{12-}$ finite chain in oxychalcogenide $Ba_6Sb_6O_2S_{13}$ leading to ultra-low thermal conductivity and giant birefringence, *Inorg. Chem. Front*., 2023, **10**, 4425–4434.

[11] M. Yang, W. D. Yao, W. Liu and S. P. Guo, The first quaternary rare-earth oxythiogermanate with second-harmonic generation and ferromagnetic behavior, *Chem. Commun*., 2023, **59**, 3894–3897.

[12] M. Sun, X. Zhang, C. Li, W. Liu, Z. Lin and J. Yao, Highly polarized $[GeOTe_3]$ motif-driven structural order promotion and an enhanced second harmonic generation

response in the new nonlinear optical oxytelluride $Ba_3Ge_2O_4Te_3$, *J. Mater. Chem*. *C,* 2022, **10**, 150–159.

[13] H. D. Yang, S. H. Zhou, M. Y. Ran, X. T. Wu, H. Lin and Q. L. Zhu, Melilite oxychalcogenide $Sr_2FeGe_2OS_6$: a phase-matching IR nonlinear optical material realized by isomorphous substitution, *Inorg. Chem. Front*., 2023, **10**, 2030.

[14] M. Sun, W. Xing, M. Lee and J. Yao, Bridging oxygen atoms in trigonal prism units driven strong second-harmonic-generation efficiency in $Sr_3Ge_2O_4Te_3$, *Chem. Commun*., 2022, **58**, 11167–11170.

[15] H.-J. Zhao, H.-D. Yang, P.-F. Liu and H. Lin, From Cc to P63mc: Structural Variation in $La_3S_2Cl_2[SbS_3]$ and $La_3OSCl_2[SbS_3]$ Induced by the Isovalent Anion Substitution, *Cryst. Growth Des*., 2022, **22**, 1437–1444.

[16] R. Wang, F. Liang, X. Zhang, Y. Yang and F. Huang, Synthesis, structural evolution and optical properties of a new family of oxychalcogenides $[Sr_3VO_4][MQ_3]$(M= Ga, In, Q= S, Se), *Inorg. Chem. Front*., 2022, **9**, 4768–4775.

[17] B. Almoussawi, W. D. Yao, S. P. Guo, M. H. Whangbo, V. Dupray, S. Clevers, S. Q. Deng and H. Kabbour, Negative Second Harmonic Response of Sn^{4+} in the Fresnoite Oxysulfide $Ba_2SnSSi_2O_7$, *Chem. Mater*., 2022, *34*, 4375–4383.

[18] N. Zhang, Q. Xu, Z. Shi, M. Yang and S. Guo, Characterizations and Nonlinear-Optical Properties of Pentanary Transition-Metal Oxysulfide $Sr_2CoGe_2OS_6$, *Inorg. Chem*., 2022, **61**, 17002–17006.

[19] W. Xing, P. Fang, N. Wang, Z. Li, Z. Lin, J. Yao, W. Yin and B. Kang, Two Mixed-Anion Units of $[GeOSe_3]$ and $[GeO_3S]$ Originating from Partial Isovalent Anion Substitution and Inducing Moderate Second Harmonic Generation Response and Large Birefringence, *Inorg. Chem*., 2020, **59**, 16716–16724.

[20] R. Wang, F. Liang, X. Liu, Y. Xiao, Q. Liu, X. Zhang, L. M. Wu, L. Chen and F.

Huang, Heteroanionic Melilite Oxysulfide: A Promising Infrared Nonlinear Optical Candidate with a Strong Second-Harmonic Generation Response, Sufficient Birefringence, and Wide Bandgap, *ACS Appl. Mater. Interfaces*, 2022, **14**, 23645–23652.

[21] M. Y. Ran, Z. J. Ma, H. Chen, B. X. Li, X. T. Wu, H. Lin and Q. L. Zhu, Partial Isovalent Anion Substitution to Access Remarkable Second-Harmonic Generation Response: A Generic and Effective Strategy for Design of Infrared Nonlinear Optical Materials, *Chem. Mater.*, 2020, **32**, 5890–5896.

[22] B. Liu, X. Jiang, G. Wang, H. Zeng, M. Zhang, S. Li, W. Guo and G. Guo, Oxychalcogenide $BaGeOSe_2$: Highly Distorted Mixed-Anion Building Units Leading to a Large Second-Harmonic Generation Response, *Chem. Mater*. 2015, **27**, 8189–8192.

[23] J. Xu, K. Wu, Y. Xiao, B. Zhang, H. Yu and H. Zhang, Mixed-AnionOriented Design of $LnMGa_3S_6O$ (Ln = La, Pr, and Nd; M = Ca and Sr) Nonlinear Optical Oxysulfides with Targeted Property Balance, *ACS Appl. Mater. Inter.*, 2022, **14**, 37967-37974.

[24] S. Cui, H. Wu, Z. Hu, J. Wang, Y. Wu and H. Yu, The Antiperovskite-Type Oxychalcogenides $Ae_3Q[GeOQ_3]$ (Ae = Ba, Sr; Q = S, Se) with Large Second Harmonic Generation Responses and Wide Band Gaps, *Adv. Sci*., 2022, **10**, 2204755.

[25] S. H. Zhou, M. Y. Ran, W. Wei, A. Y. Wang, X. T. Wu, H. Lin and Q. L. Zhu, Heteroanion-introduction-driven birefringence enhancement in oxychalcogenide $Ba_3M^{II}Ge_3O_2S_8$ (M^{II} = Mn, Cd), *Inorg. Chem. Front.*, 2023, **10**, 5997–6004.

[26] J. K. Wang, Y. S. Cheng, H. P. Wu, Z. G. Hu, J. Y. Wang, Y. C. Wu and H. W. Yu, $Sr_3[SnOSe_3][CO_3]$: A Heteroanionic Nonlinear Optical Material Containing Planar p-conjugated $[CO_3]$ and Heteroleptic $[SnOSe_3]$ Anionic Groups, *Angew. Chem.,*

Int. Ed., 2022, **61**, e202201616.

[27] M. Y. Ran, S. H. Zhou, B. Li, W. Wei, X. T. Wu, H. Lin and Q. L. Zhu, Enhanced Second-Harmonic-Generation Efficiency and Birefringence in Melilite Oxychalcogenides $Sr_2MGe_2OS_6$ (M = Mn, Zn, and Cd), *Chem. Mater.*, 2022, **34**, 3853–3861.

[28] Y. Cheng, H. Wu, H. Yu, Z. Hu, J. Wang and Y. Wu, Rational Design of a Promising Oxychalcogenide Infrared Nonlinear Optical Crystal, *Chem. Sci.*, 2022, **13**, 5305–5310.

[29] J. N. Li, X.H. Li, Y. X. Xu, W. L. Liu and S. P. Guo, First Investigation of Nonlinear Optical Oxychalcogenide with Three-Dimensional Anionic Framework and Special Windmill−Like Functional Motifs, *Chin. J. Chem*., 2022, **40**, 2407–2414

[30] Y. Shi, Z. Ma, B. Li, X. Wu, H. Lin and Q. Zhu, Phase matching achieved by isomorphous substitution in IR nonlinear optical material $Ba_2SnSSi_2O_7$ with an undiscovered [SnO_4S] functional motif, *Mater. Chem. Front*., 2022, **6**, 3054–3061.

[31] M. Y. Ran, S. H. Zhou, W. Wei, B. Li, X. T. Wu, H. Lin and Q. L. Zhu, Rational Design of a Rare-Earth Oxychalcogenide $Nd_3[Ga_3O_3S_3][Ge_2O_7]$ with Superior Infrared Nonlinear Optical Performance, *Small*, 2023, **19**, 2300248.

[32] H. Yang, S. Zhou, M. Ran, X. Wu, H. Lin and Q. Zhu, Oxychalcogenides as Promising Ultraviolet Nonlinear Optical Candidates: Experimental and Theoretical Studies of $AEGeOS_2$ (AE = Sr and Ba), *Inorg. Chem*., 2022, **61**, 15711–15720

[33] H. Liu, Z. Song, H. Wu, Z. Hu, J. Wang, Y. Wu and H. Yu, $[Ba_2F_2][Ge_2O_3S_2]$: An Unprecedented Heteroanionic Infrared Nonlinear Optical Material Containing Three Typical Anions, *ACS Mater. Lett*., 2022, **4**, 1593–1598.

[34] H. Yan, Y. Matsushita, K. Yamaura and Y. Tsujimoto, $La_3Ga_3Ge_2S_3O_{10}$: An Ultraviolet Nonlinear Optical Oxysulfide Designed by Anion-Directed Band Gap

Engineering, *Angew. Chem., Int. Ed*., 2021, **60**, 26561–26565.